Journal of Physics and Chemistry of Solids 125 (2019) 74–79

Contents lists available at ScienceDirect

Journal of Physics and Chemistry of Solids

journal homepage: www.elsevier.com/locate/jpcs

Investigation of cyclotron-phonon resonance in monolayer molybdenum disulfide

N.V.Q. Binh[a], Bui D. Hoi[b], Doan V. Thuan[c], Nguyen N. Hieu[a], Chuong V. Nguyen[d], Huynh V. Phuc[e], Tong S. Tien[f], Nguyen T.T. Nhan[g], Nguyen D. Hien[h], Nguyen N. Anh[b], Le T. Dung[b], Le T.T. Phuong[i,*]

[a] Institute of Research and Development, Duy Tan University, 03 Quang Trung, Da Nang, Viet Nam
[b] Department of Physics, University of Education, Hue University, Hue City, Viet Nam
[c] NTT Institute of Hi-Technology, Nguyen Tat Thanh University, Ho Chi Minh City, Viet Nam
[d] Department of Materials Science and Engineering, Le Quy Don Technical University, Ha Noi, Viet Nam
[e] Division of Theoretical Physics, Dong Thap University, Dong Thap, Viet Nam
[f] Department of Basic Science, University of Fire Fighting and Prevention, No. 243, Khuat Duy Tien, Thanh Xuan Dist., Ha Noi, Viet Nam
[g] Faculty of Physics, University of Science, Vietnam National University, No. 334, Nguyen Trai Str., Thanh Xuan Dist., Ha Noi, Viet Nam
[h] Nha Trang National Ethnic Minority Pre-university, Nha Trang City, Khanh Hoa Province, Viet Nam
[i] Center for Theoretical and Computational Physics, University of Education, Hue University, Hue City, Viet Nam

ARTICLE INFO

Keywords:
Optical absorption
Cyclotron resonance
Molybdenum disulfide
Electron–phonon interaction

ABSTRACT

Transition-metal dichalcogenide monolayers recently have attracted much attention motivated by their exotic physical properties. In this paper, we theoretically investigate the optical absorption in the monolayer MoS_2 which is subjected to a uniform static magnetic field and an electromagnetic wave. The magneto-optical absorption power (MOAP) is calculated using the projection operator technique in the linear response scheme, taking account of the electron–optical phonon interaction at high temperature. Both phonon emission and phonon absorption processes are included. The cyclotron–phonon resonance (CPR) is observed in the photon energy dependence of the MOAP. Numerical analyses show that the photon energy satisfying CPR condition depends linearly on the strength of magnetic field, which is similar to that in conventional low-dimensional semiconductors but different from that in graphene. The increase of the full width at half maximum (FWHM) of CPR peaks with increasing magnetic field shows a similar behaviour to that in graphene. In addition, FWHM increases slightly with temperature, which is different from that in graphene where the FWHM is temperature independent. Our investigation provides basic information about the magneto-optical properties of the monolayer MoS_2 that are useful for further experiments and applications.

1. Introduction

The discovery of graphene about a decade ago marked the beginning of the era of atomic monolayers and their heterostructures. These novel two-dimensional (2D) materials possess numerous exotic physical properties not found in conventional low-dimensional structures, making them potential candidates for future nano-electronic devices. For example, the carriers in a single-layer graphene are massless Dirac fermions moving at very high speed, about 1/300 of the speed of light [1–3]. This results in a very high carrier mobility in graphene, about 2.10^5 cm^2/V.s at room temperature [3]. However, graphene can not be implemented in optoelectronic devices as it is because of the lack of its band gap. Therefore, in parallel with studying and developing graphene-based applications, researchers have been investigating novel layered materials and their heterostructures [4–17], each structure having its own physical characteristics, suitable for specific applications. A typical example of graphene-like 2D family is transition-metal dichalcogenide (TMD) monolayers having formula MX_2 with M and X being, respectively, a transition metal (Mo, W) and a dichalcogenide (S, Se, Te) element. In general, TMD monolayers have a specified band gap, overcoming the disadvantage of the single-layer graphene whose band gap is zero. One of the first TMD monolayers to be successfully created and widely studied was molybdenum disulfide (MoS_2) monolayers. The monolayer MoS_2 has a high on/off current ratio () [18] and high carrier mobility of ~ 200 cm^2/V.s at room temperature [19,20] allowing it a potential material for novel field-effect transistors (FETs) and

* Corresponding author.
E-mail address: thuphuonghueuni@gmail.com (L.T.T. Phuong).

https://doi.org/10.1016/j.jpcs.2018.10.007
Received 24 August 2018; Received in revised form 30 September 2018; Accepted 6 October 2018
Available online 09 October 2018

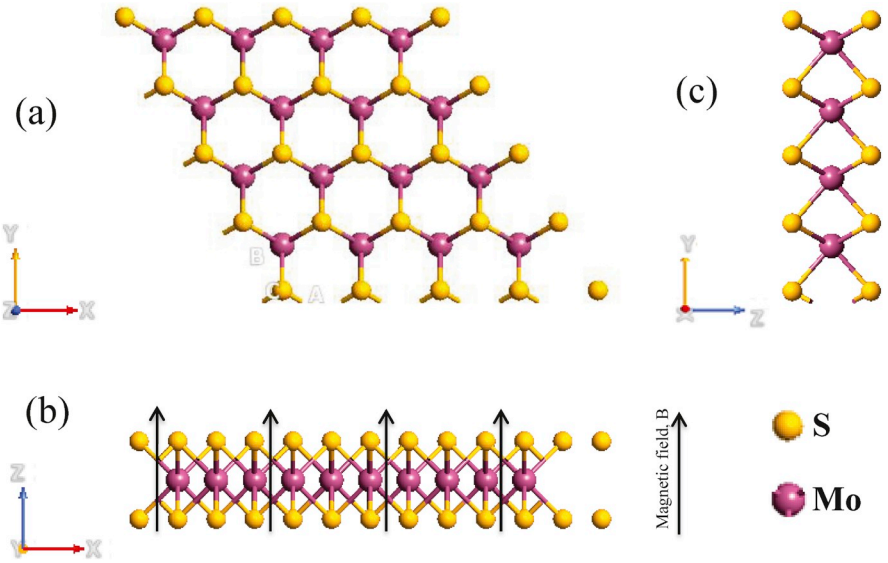

Fig. 1. The atomic structure of MoS_2 monolayer with the top view (a) and side views (b, c). Mo and S atoms are modeled, respectively, by the violet and yellow balls. Fig. 1(b) shows the MoS_2 monolayer in a uniform static magnetic field which is considered in the present calculation.

photodetectors. In addition, the MoS_2 monolayer is a buckling structure in which Mo atoms and S atoms do not locate in the same plane as shown in Fig. 1. This asymmetric arrangement opens a finite energy band gap of ~ 1.8 eV in the material at the equilibrium state [21]. Moreover, this band gap can be adjusted by changing some parameters such as strain, applied electric field, layer thickness, and so on. The asymmetry over its plane also leads to the strong spin-orbit interaction in MoS_2 which opens possible applications to spintronics.

Studying of resonant effects related to interaction of carriers, such as electron–phonon, electron–impurity interaction leads to structural information of the materials including the carrier effective mass, the distance between energy subbands, the phonon energy, and so on. Therefore, resonant effects such as magnetophonon resonance, cyclotron resonance in bulk materials in general, and in low-dimensional structures in particular, have been numerously investigated for the past decades [22–35]. Theoretically, up to date there has been no formula determining the full width at half maximum (FWHM) or half width at half maximum (HWHM) of a resonant peak. It has been shown by T. C. Phong and co-workers that the FWHM/HWHM can be extracted from the graph describing the dependence of absorption power (AP) or absorption coefficient (AC) on the photon energy. In their works, the authors proposed the so-called profile method to determine the FWHM/HWHM by computational program. The obtained results are consistent with previous theoretical predictions and available measurements [36]– [40]. Recently, some theoretical studies on the transport properties in MoS_2 monolayers in external electromagnetic fields have been carried out [18,41–43]. By using a direct relation between the absorption coefficient and transition probability of 2D electrons, Bhargavi et al. [18] calculated the optical AC in an *n*-type monolayer MoS_2 and other TMDs, taking account of the piezoelectric (PE) and deformation potential (DP) electron–acoustic phonon coupling regime. The results show that for both unscreened PE and DP coupling regime, the absorption coefficient is independent on the carrier effective mass. This behaviour is different from that in bulk semiconductors. In the work by Wang and Lei [41], the authors studied the linear magnetotransport in a monolayer MoS_2 by calculating the magnetoresistance for electron–phonon and electron–impurity interactions at high and low temperatures, respectively. The spin-orbit interaction was also included. The Shubnikov de Haas (SdH) oscillations were observed at low temperature. At high temperature, both optical phonons and acoustic phonons contribute to the magnetophonon resonances which emerge for a suspended system with high mobility. Moreover, for the electron–optical phonon (OP) interaction, a beating pattern of magnetophonon resonance was observed. In another work [42] Tahir et al. used linear response formulae to calculate the longitudinal and Hall conductivity/resistivity in a MoS_2 monolayer subjected to a perpendicular magnetic field (B). The spin and valley Zeeman effects were taken into account. The authors showed that these effects lead to new quantum Hall plateaux and new peaks in the dependence of the longitudinal resistivity on magnetic field. The presence of magnetic field results in a significant enhancement of the spin splitting as well as in a beating of the SdH oscillations at low B. The spin and valley polarisations were also investigated for the magnetic field up to 30 T. At low fields, the spin and valley polarisation show a similar behaviour whereas they are strongly separated in high-field regime. Very recently, Chuong et al. [43] have studied theoretically transport properties of a monolayer MoS_2 laid on some polar substrates in a perpendicular B and a light wave. The authors calculated the magneto-optical AC by including interaction of carriers with intrinsic acoustic and optical phonons, and surface optical phonons induced by the polar substrates. The FWHM was shown to increase with increasing magnetic field. Also, the effects of different substrates on the AC and the FWHM were compared and discussed in details. However, to our knowledge, experimental measurements of the cyclotron resonance line-width in MoS_2 monolayers have not yet been carried out. Therefore, systematic studies on the optical absorption and FWHM in this structure using different methods are currently necessary for future experiments and applications.

In this work, we investigate the magneto-optical absorption in MoS2 monolayers stimulated simultaneously by a perpendicular static magnetic field and an electromagnetic wave (EMW). By using projection operator technique, we calculate the AP taking account of the electron–OP interaction at high temperature. Both phonon emission and phonon absorption processes are considered. The AP is numerically evaluated and plotted to clarify resonant effects from absorption spectra. The paper is organised as follows. In Sec. 2, we introduce the theoretical model and basic formulae for the calculation. The brief derivation of the AP for electron–OP interaction is introduced in Sec. 3. Sec. 4 presents the numerical results and discussion. Finally, the main conclusions are shown in Sec. 5.

2. Basic formulation

In this calculation, we deal with a monolayer MoS_2 crystal with its

2D lattice plane being the (x, y) plane, as shown in Fig. 1. The electronic band structure of the material without external electromagnetic fields, has been investigated previously using tight-binding and first principle calculations [44–48]. We now apply a static magnetic field $(\vec{B})$ perpendicularly to the lattice plane (Fig. 1(b)) and choose the corresponding vector potential to be $\vec{A} = (-By, 0)$ in the Landau gauge. Then, the expression for the energy of a carrier at state $|\alpha\rangle$ is written as [41,42]

$$E_\alpha \equiv E_{n,s,\eta,\tau} = s\tau\bar{\lambda} + \eta\sqrt{\bar{\Delta}_{s\tau}^2 + n(\hbar\omega_c)^2}, \tag{1}$$

for the Landau level (LL) index $n = 1,2,3, ...$, $\bar{\Delta}_{s\tau} = \bar{\Delta} - s\tau\bar{\lambda}$, $\bar{\Delta} = \Delta/2$, $\bar{\lambda} = \lambda/2$ where Δ and λ are, respectively, the band gap and the spin-orbit coupling (SOC) energy in the monolayer MoS_2, $\tau = 1\ (-1)$ is for K (K') valley, the band index $\eta = 1\ (-1)$ represents the conduction (valence) band, the index $s = 1\ (-1)$ refers to spin up (down), and the cyclotron energy $\hbar\omega_c = at\sqrt{2}/a_c$ with $a_c = (\hbar/eB)^{1/2}$, t, and a being, respectively, the radius of electron orbit, the hopping integral, and the lattice constant.

The eigenvalue for the case of $n = 0$ is given separately to be

$$E_{0,s,\tau} = -\tau(\bar{\Delta} - s\bar{\lambda}) + s\bar{\lambda}. \tag{2}$$

We can expand the square root in Eq. (1) and simplify to have a simpler eigenvalue [43]

$$E_{n,s,\eta,\tau} = (1-\eta)s\tau\bar{\lambda} + \eta\bar{\Delta} + n\eta\frac{\hbar^2\omega_c^2}{2\bar{\Delta}_{s\tau}}, \tag{3}$$

where we have used the fact that $\hbar\omega_c \ll \bar{\Delta}_{s\tau}$. For example, for $B = 5$ T one has $\hbar\omega_c \approx 0.0433$ eV whereas the minimum value of $\bar{\Delta}_{s\tau}$ is $\bar{\Delta}_{s\tau} = \Delta/2 - \lambda/2 \approx 0.7925$ eV based on the values of λ and Δ reported in Ref. [49]. The expression (3) now exhibits a linear dependence of the Landau energy levels on the magnetic field strength B and level index n in the monolayer MoS_2, similarly to conventional 2D quantum wells and superlattices.

The corresponding eigenfunctions, including zero level ($n = 0$) have the form for the K valley and K' valley, respectively [41]

$$\psi_{n,s}^{\eta,+1}(r, k_x) = \frac{e^{ik_x x}}{\sqrt{\Theta_{n,s}^{\eta,+1}}}\begin{pmatrix}\Lambda_{n,s}^{\eta,+1}\phi_{n-1}(y-y_0)\\ \phi_n(y-y_0)\end{pmatrix}, \tag{4}$$

$$\psi_{n,s}^{\eta,-1}(r, k_x) = \frac{e^{ik_x x}}{\sqrt{\Theta_{n,s}^{\eta,-1}}}\begin{pmatrix}\phi_n(y-y_0)\\ \Lambda_{n,s}^{\eta,-1}\phi_{n-1}(y-y_0)\end{pmatrix}, \tag{5}$$

here, k_x is the component along the x-direction of electron wave vector, $\Theta_{n,s}^{\eta,\tau} = (\Lambda_{n,s}^{\eta,\tau})^2 + 1$, and $\Lambda_{n,s}^{\eta,\tau} = \sqrt{n}\hbar\omega_c/(\bar{\Delta} - \tau s\bar{\lambda}) - \eta\tau\sqrt{(\bar{\Delta} - \tau s\bar{\lambda})^2 + n\hbar^2\omega_c^2}$ and $\phi_n(y - y_0)$ represents the harmonic oscillator eigenfunction, centered at $y_0 = a_c^2 k_x$ giving by

$$\phi_n(y-y_0) = \frac{1}{\sqrt{2^n n! a_c\sqrt{\pi}}}\exp\left[-\frac{(y-y_0)^2}{2a_c^2}\right]H_n\left(\frac{y-y_0}{a_c}\right), \tag{6}$$

with $H_n(x)$ the Hermite polynomial of order n.

We now consider the propagation of an EMW with the amplitude E_0 and frequency ω in the above-mentioned MoS_2 monolayer. The interaction of electrons with photons and lattice phonons is assumed to be the unique cause that induces electron transition between Landau magnetic subbands. The AP is given by Ref. [50]

$$P(\omega) = (E_0^2/2)\mathrm{Re}\{\sigma_{+-}(\omega)\}, \tag{7}$$

in which the symbol "Re" implies "the real part of", $\sigma_{+-}(\omega)$ is the optical conductivity. According to the Kubo formalism in Ref. [51], one has

$$\mathrm{Re}\{\sigma_{+-}(\omega)\} = \frac{1}{\omega_c}\sum_\alpha \frac{|j_\alpha^+|^2(f_\alpha - f_{\alpha+1})B_\alpha(\omega)}{[\hbar\omega - (E_{\alpha+1} - E_\alpha)]^2 - B_\alpha^2(\omega)}. \tag{8}$$

Here, j_α^+ is the current matrix element, $j_\alpha^+ = \langle\alpha + 1|j^+|\alpha\rangle$ with being the one-particle current operator given by $j^+ = j_x + ij_y$. $f_\alpha = f(E_{n,s,\eta,\tau})$ is the Fermi-Dirac distribution corresponding to the state $|\alpha\rangle$ with the notice that the LL index pertinent to the fermi energy E_F is larger for the lower fields B and the bandwidth is smaller for higher LLs. Hence, one can remove the k_x dependence from the Fermi-Dirac function. The collision factor $B_\alpha(\omega)$, sometimes referred as the line-shape function is determined by the scattering mechanism. We can recast it after calculating the interaction matrix elements as

$$\begin{aligned}B_\alpha(\omega) = \frac{\pi}{\hbar(f_\alpha - f_{\alpha+1})}\Big\{&\sum_{\vec{q}}\sum_{\beta\neq\alpha+1}|g_q^\lambda|^2|J_{\alpha\beta}(q)|^2 g(\theta)g_v g_s\big[W_L^{(+)}(\alpha,\beta)\\ &- W_R^{(-)}(\beta,\alpha) + W_L^{(-)}(\alpha,\beta) - W_R^{(+)}(\beta,\alpha)\big]\\ &+ \sum_{\vec{q}}\sum_{\beta\neq\alpha}|g_q^\lambda|^2|J_{\alpha\beta}(q)|^2 g(\theta)g_v g_s\big[W_L^{(+)}(\beta,\alpha+1)\\ &- W_R^{(-)}(\alpha+1,\beta)\\ &+ W_L^{(-)}(\beta,\alpha+1) - W_R^{(+)}(\alpha+1,\beta)\big]\Big\}.\end{aligned} \tag{9}$$

where $g_v = 2$ and $g_s = 2$ represents, respectively, the degeneracy of valleys and spins, $g(\theta) = cos^2(\theta/2)$ is the overlap integral of spinor wave function, g_q^λ is the matrix element of electron–phonon coupling governed by the coupling mechanism [18,41,43,52], $|J_{\alpha\beta}(q)|$ is considered as the form factor. The terms $W_{L(R)}^{(\pm)}(\alpha,\beta)$ are as follows

$$\begin{aligned}W_L^{(\pm)}(\alpha,\beta) = \left(N_{q,\lambda} + \frac{1}{2} \pm \frac{1}{2}\right)f_\alpha(1-f_\beta)\delta(\hbar\omega + E_\alpha - E_\beta\\ \mp \hbar\omega_{q,\lambda})\delta_{k_x,k'_x\pm q_x},\end{aligned} \tag{10}$$

$$\begin{aligned}W_R^{(\pm)}(\alpha,\beta) = \left(N_{q,\lambda} + \frac{1}{2} \pm \frac{1}{2}\right)f_\alpha(1-f_\beta)\delta(-\hbar\omega + E_\alpha - E_\beta\\ \mp \hbar\omega_{q,\lambda})\delta_{k_x,k'_x\pm q_x}.\end{aligned} \tag{11}$$

where $N_{q,\lambda}$ is the distribution function for phonons of the frequency $\omega_{q,\lambda}$. $W_{L(R)}^{+}(\alpha,\beta)$ ($W_{L(R)}^{-}(\alpha,\beta)$) describes the electron transition from the state $|\alpha\rangle$ to the state $|\beta\rangle$ assisted by phonon emission (absorption).

In Eq. (9), eight terms inside the bracket, {...}, on the right hand side can be labelled, respectively, as A, B, C, D, E, F, G, H. The term A represents the transition from $|\alpha\rangle$ to $|\beta\rangle$ by emitting a phonon, whereas the term B implies the similar transition by absorbing a phonon. All rest terms (C, D, E, F, G, H) can be understood similarly. The delta functions and the Knonecker indices in Eqs. (10) and (11) enforce the energy-momentum conservation, which shows the resonant behaviour of electron–phonon–photon scattering in MoS_2 as a consequence of the selection rule.

Since the K and K' valleys are equivalent [43], so in this calculation we consider only intravalley transitions ($\tau = \tau'$), i.e, the processes taking place within the K or K' valley. Then, the form factor $|J_{\alpha\beta}(q)|$ is given by Ref. [41]

$$|J_{\alpha,\beta}(u)|^2 = \frac{\delta_{s,s'}}{\Theta_{n,s}^{\eta,\tau}\Theta_{n',s'}^{\eta',\tau}}\frac{n_1!}{n_2!}u^{n_2-n_1}e^{-u}\left[\Lambda_{n,s}^{\eta,\tau}\Lambda_{n',s'}^{\eta',\tau}\sqrt{\frac{n_2}{n_1}}L_{n_1-1}^{n_2-n_1}(u) + L_{n_1}^{n_2-n_1}(u)\right]^2, \tag{12}$$

with $L_n^m(u)$ being the associated Laguerre polynomials, $u = a_c^2 q^2/2$, $n_1 = \min(n, n')$, and $n_2 = \max(n, n')$.

3. Magneto-optical absorption power for electron–optical phonon interaction

To obtain the AP explicitly, we need to calculate $B_\alpha(\omega)$ given by Eq. (9). In MoS_2 monolayer, the square of the matrix element g_q^λ, for the coupling of electrons with intrinsic phonons, is determined as [18,52]

$$|g_q^\lambda|^2 = \frac{\hbar}{2S\rho\omega_{q,\lambda}}|M_{q,\lambda}|^2, \tag{13}$$

where ρ is the 2D density of mass of the material, S is the normalisation area, $M_{q,\lambda}$ is a matrix element determined by the coupling mechanism and the λ phonon mode.

In the following, we consider only electron–OP interaction at high temperatures. Then, in the deformation potential regime and the limit

of the zero-order of interaction, we have [46]

$$|g_q^{\lambda}|^2 = \frac{\hbar}{2S\rho\omega_0}(D_\lambda^0)^2, \tag{14}$$

where we have assumed that optical phonons are dispersionless so that $\omega_{q,\lambda} = \omega_0 =$ constant and $N_{q,\nu} \equiv N_0$. D_λ^0 is the optical deformation constant which is taken to be independent on q in this calculation. It should be noted that electron–phonon scattering contributes to the absorption coefficient by causing the change in the initial orbit of electrons. We can evaluate this contribution by converting the sums over q, β into the integrals $(S/4\pi^2a_c^2)\int_0^{2\pi} d\theta \int_0^{\infty} du$, $(L_x/2\pi)\sum_{n',s',\eta',\tau'}\int_0^{L_y/a_c^2} dk_x$ and using the orthogonality of the Laguerre polynomials. After a straightforward calculation, we obtain the explicit expressions of the terms A to H, and followed by $B_\alpha(\omega)$ and the AP. For instance, the first term (A) in Eq. (9) is obtained as

$$A = \sum_{\vec{q}}\sum_{\beta\neq\alpha+1}|g_q^{\lambda}|^2|J_{\alpha\beta}(q)|^2 g(\theta) g_\nu g_s W_L^{(+)}(\alpha,\beta)$$
$$= \Gamma\sum_{n'\neq n+1}\sum_{s',\eta',\tau'} I_{n,s,\eta,\tau}^{n',s',\eta',\tau}(1+N_0) f(E_{n,s,\eta,\tau})(1-f(E_{n',s',\eta',\tau}))\delta(X_{\alpha,\beta}^{-}), \tag{15}$$

where we have set $\Gamma = (D_\lambda^0)^2\hbar S g_s g_\nu/(16\rho\omega_0\pi^2a_c^4)$ and

$$X_{\alpha,\beta}^{-} = \hbar\omega + E_{n,s,\eta,\tau} - E_{n',s',\eta',\tau} - \hbar\omega_0, \tag{16}$$

$$I_{n,s,\eta,\tau}^{n',s',\eta',\tau} = \frac{\delta_{s,s'}}{\Theta_{n,s}^{\eta,\tau}\Theta_{n',s'}^{\eta',\tau}}\left[\left(\Lambda_{n,s}^{\eta,\tau}\Lambda_{n',s'}^{\eta',\tau}\right)^2 + 1\right]. \tag{17}$$

The delta function in Eq. (3) will be divergent when its argument is equal to zero. We now phenomenologically replace this function by the Lorentzian [53] with the width parameter $\gamma_{\alpha,\beta}^{\pm}$, namely,

$$\delta(X_{\alpha,\beta}^{\pm}) = \left(1/\pi\right)\hbar\gamma_{\alpha,\beta}^{\pm}/\left[\left(X_{\alpha,\beta}^{\pm}\right)^2 + \hbar^2\left(\gamma_{\alpha,\beta}^{\pm}\right)^2\right], \text{ with}$$
$$\left(\gamma_{\alpha,\beta}^{\pm}\right)^2 = \frac{(D_\lambda^0)^2 g_s g_\nu}{8\pi\hbar\rho\omega_0 a_c^2}\left(N_0 \pm \frac{1}{2} + \frac{1}{2}\right)\frac{\delta_{s,s'}}{\Theta_{n,s}^{\eta,\tau}\Theta_{n',s'}^{\eta',\tau}}\left[\left(\Lambda_{n,s}^{\eta,\tau}\Lambda_{n',s'}^{\eta',\tau}\right)^2 + 1\right]. \tag{18}$$

Seven rest terms (B, C, D, E, F, G, H) can be derived similarly to the term A to obtain the full $B_\alpha(\omega)$ as well as $P(\omega)$.

4. Numerical results and discussion

We now clarify characteristics of the absorption spectra by carrying out numerical calculations of the above analytic result for the AP, utilising specific parameters of monolayer MoS_2, which are given in Table 1. The energy levels given by Eq. (3) are adopted in the calculations. Also, the Fermi energy (E_F) appeared in the Fermi–Dirac distribution functions (f_α and f_β) is obtained from the relation between the density of states (DOS) and electron concentration n_c as [42]

$$n_c = \int_{-\infty}^{+\infty} D(E) f(E) dE = \frac{g_{s/v}}{D_0}\sum_{n,\eta,s} f(E_{n,s,\eta,\tau}), \tag{19}$$

where $D(E)$ is the DOS, $D_0 = 2\pi a_c^2$, and $f(E_{n,s,\eta,\tau}) = (1 + \exp[(E_{n,s,\eta,\tau} - E_F)/(k_B T)])^{-1}$. Eq. (19) shows that the Fermi energy

Table 1
Some parameters of the monolayer MoS_2 which are necessary for our numerical calculation.

Parameter	Symbol	Value
Lattice constant [49]	A	3.193 A
Hopping integral [49]	t	1.1 eV
Energy gap [49]	Δ	1.66 eV
SOC energy [49]	λ	75 meV
Mass density [46]	ρ	3.1×10^{-7} g.cmi^{-2}
Optical DP (K phonon) [46]	D_λ^0	2.6×10^{8} eV.cm^{-1}
Optical phonon energy [54]	$\hbar\omega_0$	42.2 meV

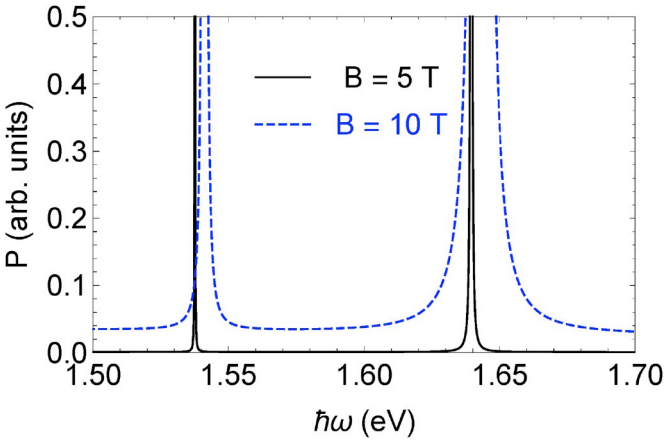

Fig. 2. The dependence of the AP on the photon energy at $B = 5$ T (solid curve) and $B = 10$ T (dashed curve). Here, $T = 200$ K.

depends on the magnetic field and temperature. In reality, however, the Fermi energy varies very weakly with the magnetic field. For example, it was shown in Ref. [42] (Figs. 3 and 4 therein) that for a wide range of magnetic field from 0 to 30 T, the Fermi energy only fluctuates between about 840 meV and 843 meV. Furthermore, we now consider only the transitions within the K valley ($\tau = \tau' = +1$). Also, all the following results are obtained for the 2D electron concentration of 5×10^{16} m^{-2}.

Fig. 2 shows the AP versus the photon energy ($\hbar\omega$) at the magnetic field of 5 T (solid curve) and 10 T (dashed curve) for the transition $(n = 1, s = +1, \eta = -1) \rightarrow (n' = 2, s' = +1, \eta' = +1)$. It can be seen clearly from the figure that, for this transition, there exist two maximum peaks on each curve. We can easily show the physical meaning of these peaks. For example, for the solid curve ($B = 5$ T) the left and the right peaks are located, respectively, at the photon energy of $\hbar\omega = 1.53764$ eV and $\hbar\omega = 1.63944$ eV and satisfy the following relations

$$E_{2,1,1,1} - E_{1,1,-1,1} - \hbar\omega_0 = \hbar\omega, \tag{20}$$

$$E_{2,1,1,1} - E_{1,1,-1,1} + \hbar\omega_0 = \hbar\omega. \tag{21}$$

So one can recognise that these resonant peaks describe the phonon-assisted cyclotron resonance or cyclotron–phonon resonance (CPR) effect, in which the left CPR peak is for phonon absorption and the right one is for phonon emission. The above CPR conditions are confirmed again in Fig. 3 where we show the AP depending on both $\hbar\omega$ and B. From Fig. 3 we can also extract the relation between the photon energy at resonance and the magnetic field. This relation is shown in Fig. 4. It

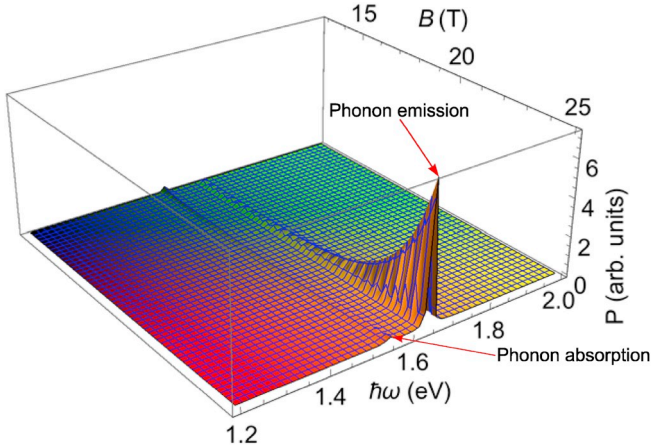

Fig. 3. Surface plot of the AP versus magnetic field and photon energy. Here, $T = 200$ K.

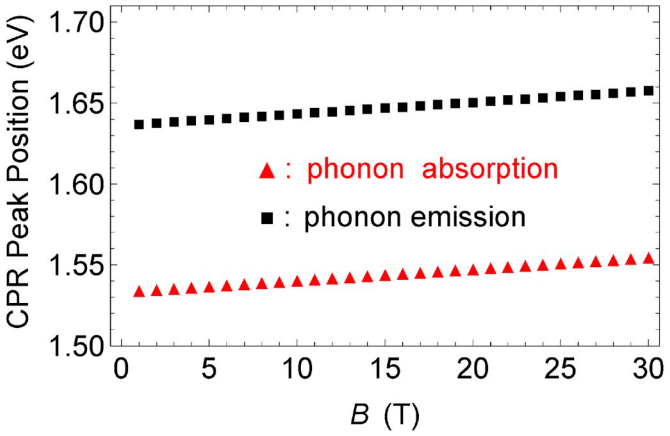

Fig. 4. The calculated CPR peak position (in the unit of energy) versus magnetic field for the same parameters as in Fig. 3.

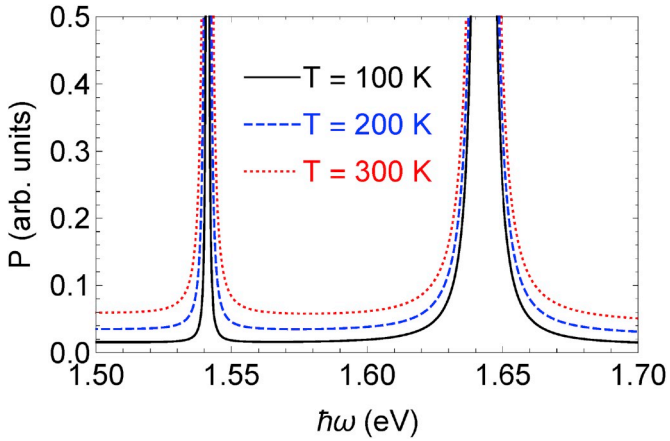

Fig. 6. The AP versus photon energy at $B = 10$ T for different values of temperature.

can be seen from Fig. 4 that the photon energy at resonance is linearly proportional to the magnetic field. In the other words, a blue-shift of CPR peaks is observed as magnetic field increases. This behaviour can be explained by the linearly magnetic field dependence of the electron energy as shown in Eq. (3). From Eq. (3) one has $\Delta E \equiv E_{2,1,1,1} - E_{1,1,-1,1} \propto B$, and according to identities (20) and (21) $\hbar\omega$ must be increased with increasing magnetic field.

To have a deeper insight about the effect of the magnetic field on the CPR in monolayer MoS_2, we now examine the dependence of the FWHM of a CPR peak on the magnetic field. Utilising the profile method [36–40], we determine the FWHM as a function of magnetic field for both phonon emission and phonon absorption processes, this dependence is shown in Fig. 5 for the temperature of 200 K. We can see from the figure that the FWHM increases with increasing magnetic field. This is because the FWHM is known to be proportional to the probability of electron–phonon interaction which is enhanced with the decrease of Landau orbits when increasing magnetic field. The increase of the FWHM with magnetic field has been observed in conventional low-dimensional semiconductors [36–38] and recently in graphene monolayers [39,40,55]. We also see from the figure that the FWHMs for phonon emission and phonon absorption differ very much from each other, especially at large magnetic field. For instance, the FWHM of CPR peak at $B = 10$ T for phonon absorption is just about one fourth of that for phonon emission. Also, the FWHM for phonon emission is always larger than that for phonon absorption at any magnetic field. Mathematically, this behaviour comes from the fact that the FWHM is proportional to the width parameter given by Eq. (18), and we can see from this equation that the width parameter for phonon emission depends on $(N_0 + 1)$ whereas it depends on N_0 for phonon absorption.

We now proceed to investigate the effect of temperature on the CPR in the monolayer MoS_2. We show again the AP as a function of photon energy in Fig. 6 at different temperatures for $B = 10$ T with the other parameters being the same with those in Fig. 2. It is seen generally that as the temperature increases, both the AP and the broadening of the CPR peaks increase. However, the temperature does not affect the CPR peak position, because the CPR conditions are governed by the delta functions which ensure the energy conservation and are independent of the temperature. The dependence of the FWHM of CPR peaks on the temperature is also shown in Fig. 7. It can be seen that the FWHMs for both phonon emission and absorption increase slightly with increasing temperature at nearly the same rate. When the temperature is increased from 10 K to 300 K, the FWHM for phonon emission/absorption process increases, respectively, from 3.39/0.106 meV to 4.99/1.69 meV. The slight increase of the FWHM with temperature in monolayer MoS_2 here is consistent with that obtained by perturbation theory for electron–OP scattering in the zero-order DP [43]. Also, this behaviour shows the difference between MoS_2 and graphene monolayers [39,40] where the FWHM remains unchanged in the same range of temperature. So far, we have not yet found any experimental measurements of the FWHM in MoS_2 monolayers to compare with the present theoretical results. However, the present investigation is of significance for further studies of magneto-optical properties of monolayer MoS_2 and potential applications of this material to future devices besides some well-known applications such as transistors [56], photodetectors [57], solar cells [58],

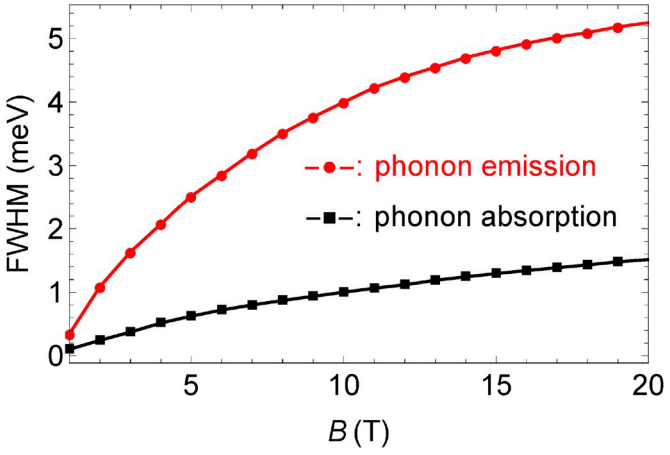

Fig. 5. The FWHM as a function of magnetic field at $T = 200$ K for phonon emission (filled circles) and phonon absorption (filled squares).

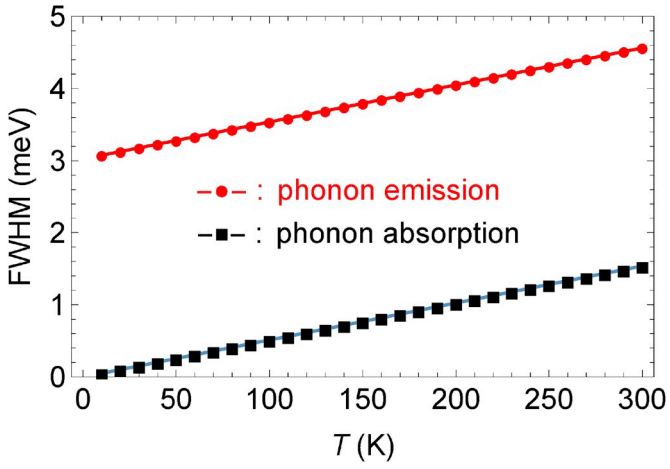

Fig. 7. Dependence of the FWHM on the temperature at $B = 10$ T.

batteries and supercapacitors for energy storage [59].

5. Conclusions

We have theoretically investigated the CPR effect in monolayer MoS_2 via the magneto-optical AP when the material is stimulated by a perpendicular magnetic field and an EMW. The main results of the present work can be summarised as follows. Based on the general formula derived by the projection operator technique, we have obtained the explicit expression for the linear AP taking into account the electron–OP interaction. The absorption spectra show CPR behaviour where the photon energy satisfying the CPR condition exhibits the blue-shift as the magnetic field increases. By using the profile method, we obtain numerically the FWHM of CPR peaks. The FWHM is found to be proportional to the strength of magnetic field in the same way as in graphene. In particular, the FWHM slightly increases with increasing temperature, showing the difference between monolayer MoS_2 and monolayer graphene. The results also show that the FWHMs for phonon emission and phonon absorption differ much from each other. Our results provide qualitatively some novel and useful information on the magneto-optical transport of the monolayer MoS_2 that may be useful for future researches and applications in nano devices.

Acknowledgement

This research is funded by Vietnam National Foundation for Science and Technology Development (NAFOSTED) under grant number 103.01-2016.83.

Appendix A. Supplementary data

Supplementary data to this article can be found online at https://doi.org/10.1016/j.jpcs.2018.10.007.

References

[1] A.H. Castro Neto, F. Guinea, N.M.R. Peres, K.S. Novoselov, A.K. Geim, Rev. Mod. Phys. 81 (2009) 109.
[2] S. Das Sarma, Shaffique Adam, E.H. Hwang, Enrico Rossi, Rev. Mod. Phys. 83 (2011) 407.
[3] K.S. Novoselov, V.I. Falko, L. Colombo, P.R. Gellert, M.G. Schwab, K. Kim, Nature 490 (2012) 192.
[4] K.S. Novoselov, A. Mishchenko, A. Carvalho, A.H. Castro Neto, Science 353 (2016) 461.
[5] A.K. Geim, I.V. Grigorieva, Nature 499 (2013) 419.
[6] M. Sun, J.P. Chou, J. Yu, W. Tang, Phys. Chem. Chem. Phys. 19 (26) (2017) 17324.
[7] M. Sun, J.P. Chou, Q. Ren, Y. Zhao, J. Yu, W. Tang, Appl. Phys. Lett. 110 (17) (2017) 173105.
[8] S. Wang, C. Ren, H. Tian, J. Yu, M. Sun, Phys. Chem. Chem. Phys. 20 (19) (2018) 13394.
[9] S. Wang, H. Tian, C. Ren, J. Yu, M. Sun, Sci. Rep. 8 (1) (2018) 12009.
[10] M. Sun, J.P. Chou, J. Yu, W. Tang, J. Mater. Chem. C 5 (39) (2017) 10383.
[11] Renato B. Pontes, Roberto H. Miwa, Antônio J.R. da Silva, Adalberto Fazzio, JosÃ©E. Padilha, Phys. Rev. B 97 (2018) 235419.
[12] J.E. Padilha, A. Fazzio, Antônio J.R. da Silva, Phys. Rev. Lett. 114 (2015) 066803.
[13] H.D. Bui, M. Yarmohammadi, Solid State Commun. 280 (2018) 39.
[14] Huynh V. Phuc, Nguyen N. Hieu, Bui D. Hoi, Chuong V. Nguyen, Phys. Chem. Chem. Phys. 20 (2018) 17899.
[15] H.D. Bui, M. Yarmohammadi, J. Magn. Magn Mater. 465 (2018) 646.
[16] M. Yarmohammadi, Solid State Commun. 250 (2017) 84.
[17] M. Yarmohammadi, J. Electron. Mater. 46 (2) (2016) 747.
[18] K.S. Bhargavi, Sukanya Patil, S.S. Kubakaddi, J. Appl. Phys. 118 (2015) 044308.
[19] Britton W.H. Baugher, Hugh O.H. Churchill, Yafang Yang, Pablo Jarillo-Herrero, Nano Lett. 13 (9) (2013) 4212.
[20] Branimir Radisavljevic, Andras Kis, Nat. Mater. 12 (9) (2013) 815.
[21] Kin Fai Mak, Changgu Lee, James Hone, Jie Shan, Tony F. Heinz, Phys. Rev. Lett. 105 (2010) 136805.
[22] J.S. Bhat, S.S. Kubakaddi, B.G. Mulimani, J. Appl. Phys. 70 (1991) 2216.
[23] A. Suzuki, D. Dunn, Phys. Rev. B 25 (1982) 7754.
[24] D. Dunn, A. Suzuki, Phys. Rev. B 29 (1984) 942.
[25] C.K. Sarkar, R.J. Nicholas, J. Phys. C Solid State Phys. 18 (1985) 1495.
[26] M.P. Chaubey, C.M. Van Vliet, Phys. Rev. B 34 (1986) 3932.
[27] R.J. Nicholas, et al., Phys. Rev. B 45 (1992) 12144(R).
[28] N.L. Kang, et al., J. Phys. Condens. Matter 7 (1995) 8629.
[29] Y.J. Cho, N.L. Kang, K.S. Bae, J.Y. Ryu, S.D. Choi, J. Phys. Condens. Matter 8 (1996) 6957.
[30] W. Xu, C. Zhang, Phys. Rev. B 54 (1996) 4907.
[31] A. Suzuki, M. Ogawa, J. Phys. Condens. Matter 10 (1998) 4659.
[32] S.C. Lee, H.S. Ahn, D.S. Kang, S.O. Lee, S.W. Kim, Phys. Rev. B 67 (2003) 115342.
[33] S.C. Lee, J. Kor. Phys. Soc. 51 (2007) 1979.
[34] X.G. Wu, F.M. Peeters, Y.J. Wang, B.D. McCombe, Phys. Rev. Lett. 84 (2000) 4934.
[35] W.Y. Wang, W. Xu, Phys. Rev. B 86 (2012) 045307.
[36] T.C. Phong, L.T.T. Phuong, H.V. Phuc, Superlattice. Microst. 52 (2012) 16.
[37] H.V. Phuc, N.T.T. Thao, L. Dinh, T.C. Phong, J. Phys. Chem. Solid. 75 (2014) 300.
[38] H.V. Phuc, N.N. Hieu, L. Dinh, T.C. Phong, Optic Commun. 335 (2015) 37.
[39] H.V. Phuc, N.N. Hieu, Optic Commun. 344 (2015) 12.
[40] B.D. Hoi, L.T.T. Phuong, T.C. Phong, J. Appl. Phys. 123 (2018) 094303.
[41] C.M. Wang, X.L. Lei, Phys. Rev. B 92 (2015) 125303.
[42] M. Tahir, P. Vasilopoulos, F.M. Peeters, Phys. Rev. B 93 (2016) 035406.
[43] Chuong V. Nguyen, Nguyen N. Hieu, Nikolai A. Poklonski, Victor V. Ilyasov, Le Dinh, Tran C. Phong, Luong V. Tung, Huynh V. Phuc, Phys. Rev. B 96 (2017) 125411.
[44] Chuong V. Nguyen, Nguyen N. Hieu, Chem. Phys. 468 (2016) 9.
[45] E. Cappelluti, R. Roldan, J.A. Silva-Guillen, P. Ordejon, F. Guinea, Phys. Rev. B 88 (7) (2013) 075409.
[46] K. Kaasbjerg, K.S. Thygesen, K.W. Jacobsen, Phys. Rev. B 85 (11) (2012) 115317.
[47] Qing Tang, Zhen Zhou, Prog. Mater. Sci. 58 (8) (2013) 1244.
[48] E.S. Kadantsev, P. Hawrylak, Solid State Commun. 152 (10) (2012) 909.
[49] Di Xiao, Gui-Bin Liu, Wanxiang Feng, Xiaodong Xu, Yao Wang, Phys. Rev. Lett. 108 (2012) 196802.
[50] A. Lodder, S. Fujita, J. Phys. Soc. Jpn. 25 (1968) 774.
[51] Y.J. Cho, S.D. Choi, Phys. Rev. B 47 (1993) 9273.
[52] K. Kaasbjerg, K.S. Thygesen, A. Jauho, Phys. Rev. B 87 (2013) 235312.
[53] M.P. Chaubey, C.M. Van Vliet, Phys. Rev. B 33 (1986) 5617.
[54] Xiaodong Li, Jeffrey T. Mullen, Zhenghe Jin, Kostyantyn M. Borysenko, M. Buongiorno Nardelli, Ki Wook Kim, Phys. Rev. B 87 (2013) 115418.
[55] Z. Jiang, E.A. Henriksen, L.C. Tung, Y.-J. Wang, M.E. Schwartz, M.Y. Han, P. Kim, H.L. Stormer, Phys. Rev. Lett. 98 (2007) 197403.
[56] B. Radisavljevic, A. Radenovic, J. Brivio, V. Giacometti, A. Kis, Nat. Nanotechnol. 6 (2011) 147.
[57] Hong Wang, Fucai Liu, Wei Fu, Zheyu Fang, Zhou Wu, Liu Zheng, Nanoscale 6 (2014) 12250.
[58] Wi Sungjin, Hyunsoo Kim, Mikai Chen, Hongsuk Nam, L. Jay Guo, Edgar Meyhofer, andXiaogan Liang, ACS Nano 8 (5) (2014) 5270.
[59] Gong Zhang, Huijuan Liu, Jiuhui Qu, andJinghong Li, Energy Environ. Sci. 9 (2016) 1190.